Correlations between structure, material properties and bioproperties in self-assembled β-hairpin peptide hydrogels

Rohan A. Hule,[a] Radhika P. Nagarkar,[b] Aysegul Altunbas,[a] Hassna R. Ramay,[a] Monica C. Branco,[b] Joel P. Schneider*[b] and Darrin J. Pochan*[a]

Received 14th November 2007, Accepted 15th January 2008
First published as an Advance Article on the web 16th May 2008
DOI: 10.1039/b717616c

A *de novo* designed β-hairpin peptide (MAX8), capable of undergoing intramolecular folding and consequent intermolecular self-assembly into a cytocompatible hydrogel, has been studied. A combination of small angle neutron scattering (SANS) and cryogenic-transmission electron microscopy (cryo-TEM) have been used to quantitatively investigate the MAX8 nanofibrillar hydrogel network morphology. A change in the peptide concentration from 0.5 to 2 wt% resulted in a denser fibrillar network as revealed *via* SANS by a change in the high q ($q = (4\pi/\lambda) \times \sin(\theta/2)$, where λ = wavelength of incident neutrons and θ = scattering angle) mass fractal exponent from 2.5 to 3 and by a decrease in the measured correlation length from 23 to 16 Å. A slope of −4 in the USANS regime indicates well-defined gel microporosity, an important characteristic for cellular substrate applications. These changes, both at the network as well as the individual fibril lengthscales, can be directly visualized *in situ* by cryo-TEM. Fibrillar nanostructures and network properties are directly related to bulk hydrogel stiffness *via* oscillatory rheology. Preliminary cell viability and anchorage studies at varying hydrogel stiffness confirm cell adhesion at early stages of cell culture within the window of stiffness investigated. Knowledge of the precise structure spanning length scales from the nanoscale up to the microscale can help in the formation of future, specific structure–bioproperty relationships when studying *in vitro* and *in vivo* behavior of these new peptide scaffolds.

Introduction

Hydrogels are a class of extensively studied materials with established applications in a multitude of biomedical areas including substance release[1–3] and soft[4–6] and hard[7–10] tissue regeneration. Some of the innate material property prerequisites for materials to be functional in these vastly varying end uses include degradation and release over specific and controllable time scales, desired mechanical properties, and porosity to enable cellular nutrient and waste diffusion and enable cell motility.[11] One of the inherent structural factors in hydrogels that explains such versatility in function is the underlying network nanostructure. Physical crosslinking (through

[a]*Department of Materials Science and Engineering and Delaware Biotechnology Institute, University of Delaware, Newark, DE, 19716. E-mail: pochan@udel.edu*
[b]*Department of Chemistry and Biochemistry, University of Delaware, Newark, DE, USA 19716. E-mail: schneijp@udel.edu*

hydrodynamic interactions,[12,13] ionic strength[14] or chain entanglements[15]) or chemical crosslinking (through triggers such as temperature[16] or photopolymerization[17,18]) are both strategies used for formation of hydrogel networks. Nanostructural features of the networks such as polymer or fibril persistence length, nature and density of crosslinks, mesh size and hydrophobic interactions directly impact properties such as bulk hydrogel stiffness, porosity, and biological features including cytotoxicity, cell viability and cell adhesion, as well as cell motility. Therefore, a thorough study of the underlying structure–bioproperty relationships in these hydrogel networks is required for designed biological usage. This paper focuses on understanding clear structure–material property relationships as well as preliminary physical–bioproperty relationships in self-assembled peptide-based hydrogels and directly relates the structure, spanning lengthscales from the nanoscale up to the microscale, to bulk material stiffness as well as potential cell adhesion and viability. Hydrogel formation occurs *via* the self-assembly of amphiphilic, short peptide sequences into well-defined nanofibrils. Being synthetically derived, these hydrogels have the added advantage of precise control over nanomorphology and functionality, allowing for the study of a single effect without interference from the remaining system. We have employed a combination of complimentary tools, namely scattering to enable a global study of the network on multiple length scales (from μm to Å) and electron microscopy to provide a direct, *in situ* visualization of the local network nanostructure. The structure, in turn, is related to bulk material stiffness evaluated using rheology and biological activity assessed by cell viability and morphology assays with MC3 T3 rat calvarial preosteoblasts.

Results and discussions

The Pochan and Schneider labs currently investigate the design and self-assembly behavior of short, synthetic peptides that undergo triggered self-assembly to form rigid hydrogel networks. The self-assembly mechanism consists of the intramolecular folding of amphiphilic β-hairpin peptides in response to specific triggers. Correct intramolecular folding leads to consequent intermolecular assembly through hydrogen bonding and hydrophobic interactions to yield fibrillar nanostructures leading to gelation. The fibrils that constitute the hydrogel network are monodisperse in width and display unique nanostructures (twisting *vs.* non-twisting *vs.* laminating), depending on the amino acid sequence.[19] Peptide design has led to the study of numerous triggers including pH,[20] temperature,[21] ionic strength[22] or light.[23] MAX1, the 20 amino-acid parent peptide used in these studies, consists of 2 strands of alternating valine (V) and lysine (K) residues flanking a central tetrapeptide type II′ β-turn region ($VKVKVKVKV^{D}PPTKVKVKVKV\text{-}NH_2$).[20] The peptide exists in a random coil conformation at pH 7.4 and low salt concentration due to the electrostatic repulsion between the positively-charged lysine residues. However, on being subjected to high pH or high salt content, some of the positive charges are deprotonated or the charge is screened inducing a facially amphiphilic β-hairpin conformation. Folded hairpins subsequently self-assemble, both laterally and facially, primarily *via* lateral intermolecular H-bonds and hydrophobic collapse of the valine-rich faces, respectively, to form fibrillar nanostructures. MAX1 gelation can be triggered by addition of cell culture media to aqueous solutions of unfolded peptide[24] thus enabling 2D and 3D cell culturing upon or within the gel scaffold. However, the slow kinetics of MAX1 gelation in *in vitro* cell culture conditions results in cell sedimentation and prevents uniform cell distribution throughout the MAX1 gel matrix. Cell distribution in 3D cell culture was improved by a single substitution of glutamic acid at position 15 on the hydrophilic face, resulting in a new peptide, MAX8 ($VKVKVKVKV^{D}PPTKVEVKVKV\text{-}NH_2$).[25] The negatively charged glutamic acid lowers the overall positive charge of the peptide and enables faster folding and self-assembly (and, consequently gelation) in cell culture environments.[25] The self-assembly mechanism for MAX8 is similar to MAX1 and is shown

in Fig. 1. As with MAX1, MAX8 gels are composed of well-defined fibrils, $\approx$ 3.2 nm in width as measured from multiple TEM micrographs.[25]

An excellent tool for quantitative, global evaluation of the MAX8 network on length scales varying from a few Å to a few hundred nanometers is small angle neutron scattering (SANS). SANS data for MAX8, with concentrations varying from 0.5 wt% through 2 wt% are shown in Fig. 2 as the scattering intensity, $I(q)$ *vs.* the scattering vector, q, where $q = (4\pi/\lambda) \times \sin(\theta/2)$, λ = wavelength of incident neutrons and θ = scattering angle. As mentioned earlier, SANS was chosen to quantify globally the hydrogel network morphology at two distinct length scales; the network morphology at 100s of nanometers and the local fibrillar nanostructure at 1–10 nanometers. Fits of the data to the following functional form were performed:

$$I(Q) = A/Q^n + C/[1 + (QL)^m] + B$$

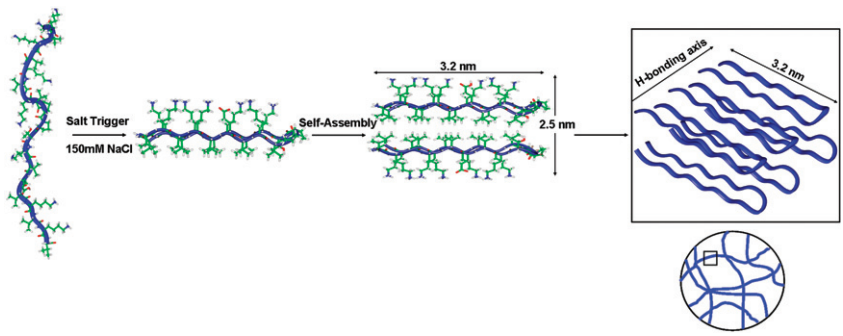

Fig. 1 Self-assembly mechanism for MAX8. Addition of the trigger (50 mM BTP, 150 mM NaCl, pH 7.4) to the unfolded peptide solution drives the unfolded peptide to adopt a β-hairpin conformation. Numerous hairpins assemble laterally, primarily due to hydrogen bonding, and facially, due to hydrophobic collapse, into a monodisperse fibrillar nanostructure. Multiple fibrils form a network, leading to hydrogel formation.

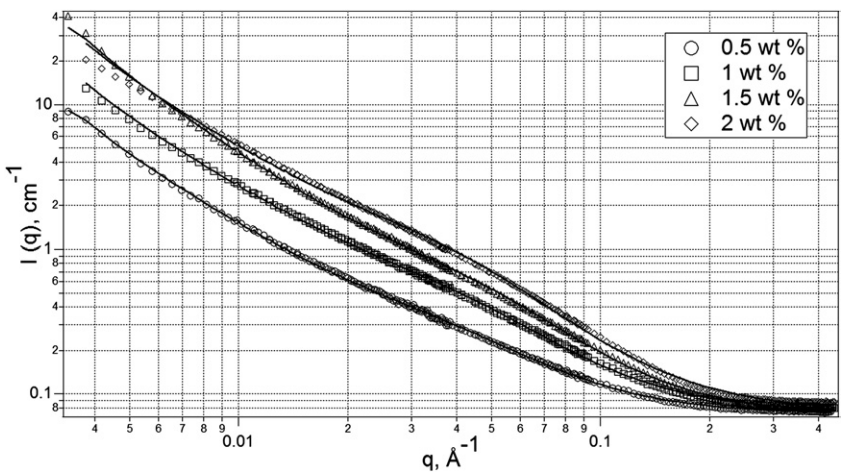

Fig. 2 SANS data for varying concentrations of MAX8 hydrogels left overnight after triggering self-assembly *via* 50 mM BTP, 150 mM NaCl, pH 7.4 at room temperature. Concentrations studied were 0.5 wt% (○), 1 wt% (□), 1.5 wt% (△) and 2 wt% (◇). The solid lines are fits to the functional form.

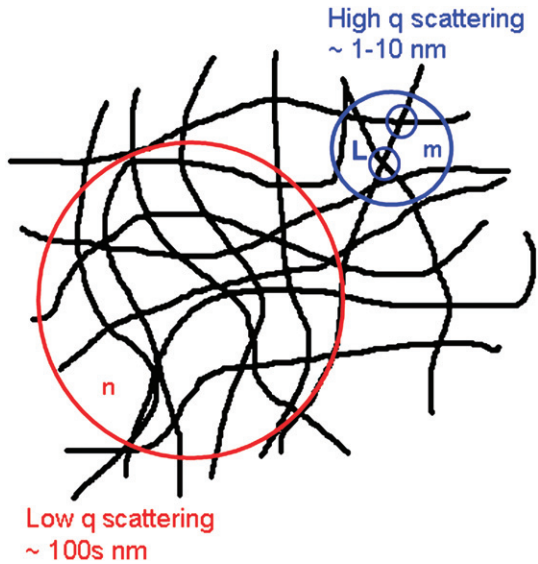

Fig. 3 A schematic of the MAX8 hydrogel network explaining the significance of various parameters extracted from the SANS data fits to the functional form. The red and blue circles represent scattering at two distinct length scales, the hydrogel network morphology at 100s of nanometers and the local nanostructure at 1–10 nanometers, respectively. Fibrillar density at these length scales is represented by the low-q and high-q scattering exponents, n and m, respectively. The distances associated with individual interfibrillar crosslinks at high q is represented by the correlation length (L).

In the above equation, network scattering in the low q regime can be described by the first term, A/Q^n and is qualitatively similar to Porod-like scattering.[26] High q scattering is expressed by the second term, $C/[1 + (QL)^m]$. This is a Lorentzian function that has been used to characterize polymer/solvent interactions and chain solvation characteristics.[27] In this paper, it identifies the fibrillar morphology and the network structure on the nanoscale. The multiplicative factors of the Porod and Lorentzian terms (A and C, respectively), the q-independent incoherent background scattering (B), the correlation length (L), and the low-q and high-q scattering exponents (n and m, respectively) were obtained by a nonlinear, least-squares fit of the data. A physical representation of the fitted parameters in terms of the MAX8 hydrogel network is shown in Fig. 3. The two circles of varying radii represent the network morphology probed by scattering in the low-q regime and the local nanostructure probed by scattering in the high-q regime. Scattering exponents in the low- and high-q regimes (n and m, respectively) can be interpreted to be representative of the fibrillar densities observed at these two distinct length scales. The correlation length at high-q, L, represents weighted-average interdistance between the fibrils, also seen as the interfibrillar crosslinking distance/mesh size-like spacing in cryo-TEM micrographs. Similar functional forms have been successfully employed to study diverse systems including clustering and solvation characteristics of polymer[28] and polyelectrolte solutions,[29] block copolypeptides[30] and other similar self-assembled hydrogel systems.[31]

The scattering profiles shown in Fig. 2 can be used to accurately depict changes in the MAX8 hydrogel network with changes in peptide concentration. A closer look at the fitted parameters reveals that the low q scattering exponent (n) does not vary significantly from 1.7 irrespective of the peptide concentration. Such exponents in the low q regime that describe the hydrogel structure across 100s of nanometers are suggestive of a homogeneous morphology of the hydrogel network at these

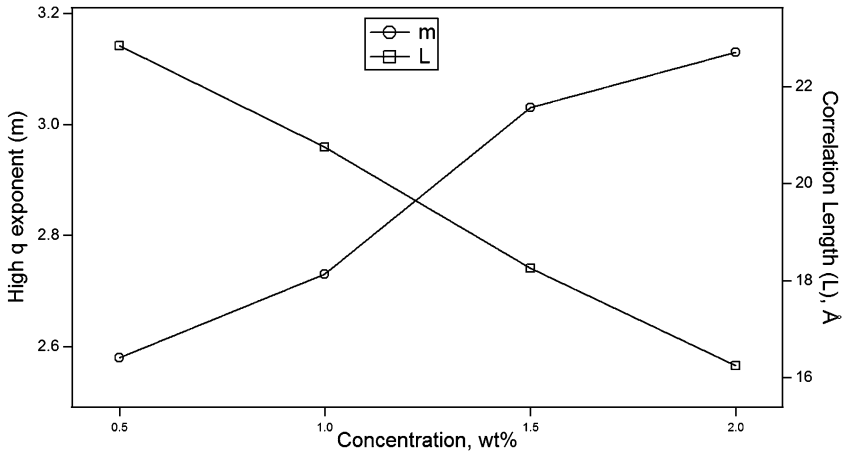

Fig. 4 Variation in m, the high-q scattering exponent (○) and L, the correlation length (□) with increasing MAX8 concentration. The increase in the high-q exponent, m, from 2.58 to 3.13 and the decrease in the correlation length, L, from 22.83 to 16.25 Å denote an increasing density of the network with concentration.

length scales. Ramachandran *et al.* have inferred a comparable homogeneous morphology on similar length scales from a mass fractal power-law decay analysis of oligopeptide hydrogels.[32] The number of fibrillar entanglement/crosslinking points increases with an increase in peptide concentration, thus making the network denser. This increase in the number of crosslinks, and, thus, scattering centers can be clearly seen as higher intensities in the mid- and low-q regimes. In the high-q regime, differences in the local network morphology (1–10 nanometers) can be tracked by the high-q scattering exponent (m) extracted from the fits to the functional form. As explained earlier in the schematic in Fig. 3, the scattering exponent is analogous to the fibrillar density at distinct length scales. As shown in Fig. 4, MAX8 has a high-q exponent of 2.58 at 0.5 wt% indicative of a mass fractal. Mass fractal[33,34] scattering occurs when $I(q) \sim S(q) \sim q^{-D_m}$ where D_m is the mass fractal dimension and has a value of 1–3. The values for the high-q exponent increase to 2.73 at 1 wt% and to 3.03 at 1.5 wt%, suggestive of the increasing compactness/density of the self-assembled fibrils that form the local network morphology. Thus, transitions in the hydrogel network can be quantitatively understood by a fractal analysis. We have performed similar analyses on other hydrogel systems and have observed changes in the fractal nature of the self-assembled network with concentration.[30,31] Similarly, Hammouda *et al.* have deduced an increasing degree of polymer chain compactness from a change in the high q exponent from 1.67 to 3.7 in other biophysical systems.[35]

Another parameter that supports the trend of increasing local network density with peptide concentration is the correlation length, L, associated with interfibril distances in the proximity of individual crosslinking points, as shown in the schematic in Fig. 3. The correlation length decreases from 23 Å at 0.5 wt% to 16 Å at 2 wt% MAX8, Fig. 4. An increase in the compactness of the network with concentration can be related to an increase in the number of crosslinks and an associated reduction in the inter-fibrillar distance at these points. This correlation length is distinct from the mesh size or pore size resulting from the average distance between distinct fibrils or between neighboring crosslink points that can be seen directly *via* cryo-TEM in the 2-D projection of the fibrillar network. We have observed a comparable variation in correlation lengths with changes in the concentration in other membranous copolypeptide-based[30] and self-assembling peptide[31] hydrogels. Similar interpretations of correlation length changes have been used to analyse DNA denaturation[35] and PEO clustering.[28] Thus, a combination of increasing fractal

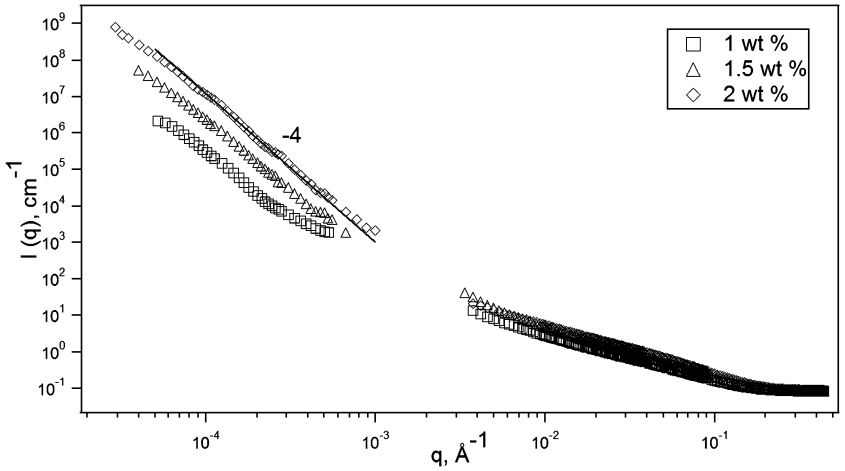

Fig. 5 Combined USANS and SANS data for a concentration series of MAX8 hydrogels shows scattering intensity decaying with a slope of −4 in the low-q regime. Such behavior, similar to Porod-like scattering, indicates the presence of sharp interfaces between the hydrogel matrix and surrounding solvent on the micron length scales and is suggestive of hydrogel being microporous. Concentrations studied were 1 wt% (□), 1.5 wt% (△) and 2 wt% (◇).

exponents within the mass fractal regime and decreasing correlation lengths points towards higher crosslinking density and smaller interfibrillar distances in the proximity of crosslink points with concentration.

Another feature apparent from the scattering data is the sharp upturn at low-q for all concentrations of MAX8. This is the result of fibrillar associations at larger length scales ($d \sim$ 100–250 nm). The extent of the low-q regime interrogated can be extended to lower values and larger spacings with ultra small angle neutron scattering (USANS), allowing us to globally quantify MAX8 hydrogel morphology between 0.6–20 microns. Combined SANS and USANS data at identical concentrations to those discussed above, shown in Fig. 5, indicate an intensity decay with a q^{-4} dependence in the USANS regime. Such power law behavior is qualitatively similar to surface fractal or Porod-like scattering, *i.e.* scattering from a sharp interface between two phases. Surface fractal[34] scattering has been expressed as $I(q) \sim S(q) \sim q^{-(6-D_s)}$ where D_s is the surface fractal dimension which ranges from 2 to 3. The extreme limit for surface fractals is a flat surface when $D_s = 2$; therefore, the slope of $I(q) \propto q^{-4}$. It is very likely that the gel matrix exhibits a sharp interface to the surrounding solvent on the micron length scale. Porod scattering has been observed, both at high-[34,36] and low-q[20,37,38] regimes, in other hydrogel systems.

The hydrogel morphology and network density at different peptide concentrations can be determined directly by cryogenic transmission electron microscopy (cryo-TEM). Cryo-TEM enables imaging of the hydrogel network under cryogenic conditions, thus preserving the *in situ* nanostructure. The gray areas seen in Fig. 6 are vitrified water, while the dark areas are self-assembled fibrils constituting the MAX8 hydrogel matrix. Cryo-TEM confirms the fibrillar nanostructures resulting from the self-assembly and the dense network that constitutes the hydrogel matrix and that serves as the origin of the mass fractal scattering as seen in SANS. Similarly, cryo-TEM reveals the increasing density of the hydrogel network from 0.5 wt% (Fig. 5A) to 2 wt% (Fig. 5B) leading to an increase in the mass fractal exponent, in excellent agreement with SANS predictions. An elevation in both the fibrillar density and the number of crosslinks with concentration brings them closer, seen directly as both a decrease in the interfibrillar distances in the proximity of crosslinks as well as the pore size spacing between fibrils in the micrographs. As explained

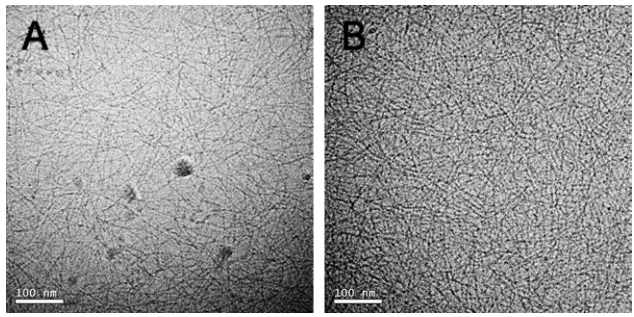

Fig. 6 Cryo-TEM micrographs of 0.5 wt% (A) and 2 wt% (B) MAX8, representing the *in situ* nanostructure of the hydrogel at varying concentrations. The increase in the fibrillar network density with concentration can be directly visualized.

earlier, the reduction in the interfibril distance associated with individual fibrillar crosslinks can be related to the decrease in the correlation length measured from fits to the SANS data.

The dependence of the fibrillar nanostructure and network properties on the bulk hydrogel stiffness was assessed by oscillatory rheology. Fig. 7 shows the frequency dependence of the elastic modulus (G') of increasing MAX8 hydrogel concentrations, from 0.5 to 2 wt%, investigated in the 0.1–100 rad s^{-1} range at 20 °C. Hydrogels were assembled on the rheometer under experimental conditions identical to scattering and electron microscopy studies. The growth in G' was tracked for 1 hour prior to a frequency sweep to ensure steady-state conditions. Increase in the G' can be attributed to a rise in non-covalent crosslinks formed between the self-assembled fibrils with time, as seen in dynamic time sweeps (data not shown). The network plateau behavior can be clearly seen in the frequency independent elastic moduli at all peptide concentrations. The solid-like characteristics of these hydrogels can be assessed by the fact that the G' values are a magnitude higher than the

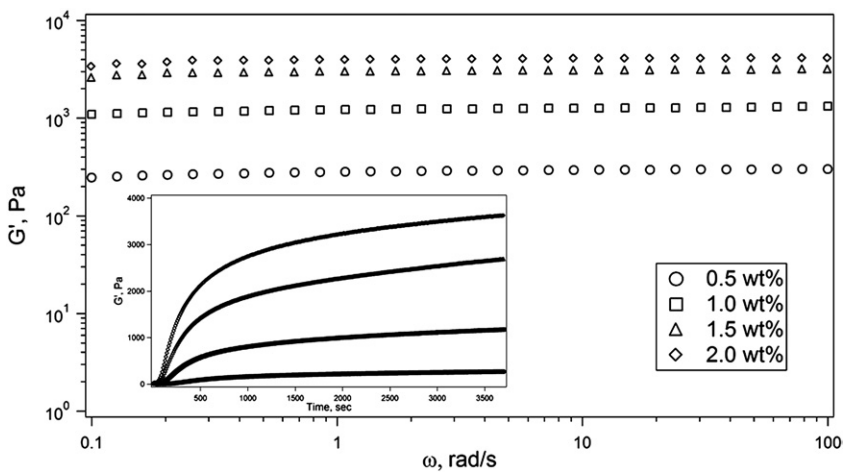

Fig. 7 Frequency sweep data showing the storage modulus (G') for 0.5 wt% (○), 1 wt% (□), 1.5 wt% (△) and 2 wt% (◇) MAX8 hydrogels at pH 7.4, 50 mM BTP buffer, 150 mM NaCl, 20 °C. Data was obtained from 3 independent experiments on 3 discreet samples and shows a standard deviation of less than 10%. The loss moduli (G'') are not shown here for sake of clarity. Inset: Dynamic time sweeps showing the growth in G' over a period of 1 hour at identical concentrations.

corresponding loss moduli (G'') for all concentrations (data not shown for sake of clarity). As seen in Fig. 7, the plateau modulus of MAX8 gels can be controllably altered from 270 ± 16 Pa at 0.5 wt% to 3600 ± 183 Pa at 2 wt%. This change observed in the stiffness of MAX8 hydrogels is directly related to the increase in the network density and the degree of crosslinks with concentration, seen earlier using SANS and cryo-TEM, respectively. It has also been shown in recent studies[25] that MAX8 hydrogels exhibit shear thinning and quick recovery of up to 90 ± 10% of the original stiffness upon cessation of shear. The fast recovery has been attributed to a substantial population of the network non-covalent crosslinks that remain intact during shear. This study proves that network morphology and the degree of non-covalent crosslinking can be directly related and can be used to tune the final modulus of these peptide-based hydrogels.

The importance of scaffold matrix mechanical properties on cell viability and adhesion has been recently well documented.[39–42] Pelham[39] *et al.* have shown that cell locomotion and adhesion can be altered by the modulus of the substrate. Cell motility was found to be directly affected by the substrate flexibility with cells on flexible substrates showing reduced spreading and elevated motility rates. It has been seen that soft, lightly crosslinked gels ($E' \sim 1$ kPa) promote diffuse and dynamic adhesion as opposed to stable focal adhesion found in stiff, highly crosslinked gels ($E' \sim 30$–100 kPa).[41] These observations are consistent with reduced adhesion strengths to overcome in order to peel off cells from soft gels *versus* glass.[43] Such studies lead to the conclusion that cells demonstrate the ability to survey the mechanical properties of their environment.

We present here preliminary results probing the effect of MAX8 hydrogel matrix stiffness (and hence network morphology) on cell viability and initial cell morphology. Fig. 8 shows laser confocal scanning microscopy (LCSM) images of MC3 T3-E1 (preosteoblast) cells cultured on the surface of MAX8 scaffolds of varying

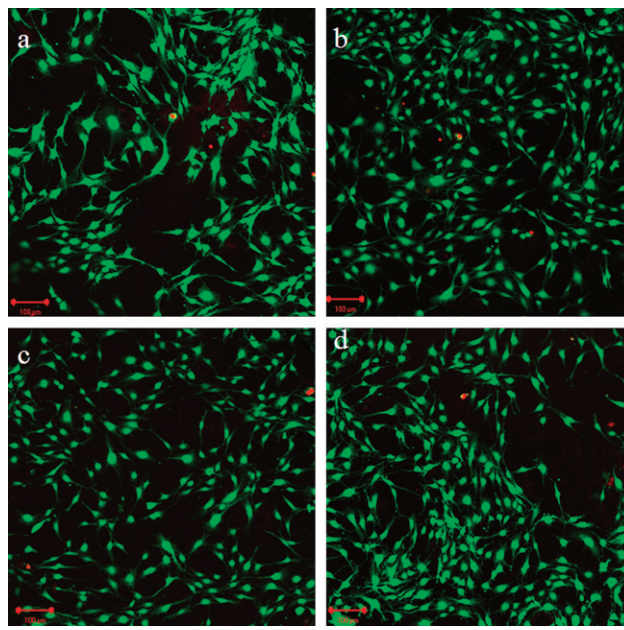

Fig. 8 Confocal microscopy images obtained during a Live/Dead assay on 0.5 wt% (a), 1 wt% (b), 1.5 wt% (c) and 2 wt% (d) MAX8 hydrogels. Live cells (stained green) from 5 randomly chosen micrographs for each sample were counted. Dead cells (stained red) were ignored since they were less than 1% in total cell count (data not shown).

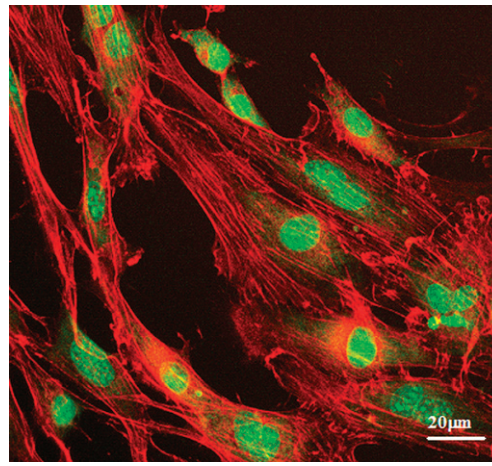

Fig. 9 Initial morphology of MC3T3 cells cultured on MAX8 hydrogel for 24 hours, characterized by actin stress fiber formation. Actin fibers are shown in red while cellular nucleus is stained green.

concentration, and thus, stiffness. Live cells have been stained green while dead cells are red. It can be clearly seen after 24 hours of cell culture on the hydrogel scaffolds that most of the cells (~99%) from 5 randomly chosen micrographs are living, irrespective of the matrix stiffness. Cells are well spread on the surface with fibroblast-like morphology indicating that cells are predominantly attached. These results demonstrate that the hydrogel scaffold is qualitatively non-cytotoxic towards pre-osteoblast cells. The cytoskeletal organization of the cells was examined by labeling F-actin microfilaments with a fluorescently labeled dye.[44] LSCM was used to observe the fluorescently labeled actin fiber organization. Fig. 9 shows the typical appearance of stressed F-actin fibers (red) and nucleus (green) of cells attached to 0.75 wt% peptide hydrogel surface. Nearly all the cells are spread and display cellular extensions in all directions on hydrogel. Thin and stretched F-actin fibers are visible in the cytoplasm. F-Actin fibers anchor the cell to the surface *via* focal adhesion complexes and apply stress to the interior of the cell. The presence and arrangement of actin filaments and focal adhesion points indicate the degree of adhesion strength and are central to adhesion signaling.[45,46] Cell signaling pathways are initiated after cell adhesion and have important consequences for cell processes such as migration and differentiation.[47,48] The stretched F-actin fibers are indicative of the attachment, cytoskeleton development and spreading of cells on hydrogel. These initial results confirm cell viability and cytoskeletal fiber development in MC3 T3 cells within a G' range of ~270–3600 Pa for the MAX8 scaffold at early stages of cell culture. Further studies are currently underway to increase the scaffold stiffness range by chemical or physical means in order to probe the mechanical responsiveness of a wide variety of mammalian cells.

Conclusions

Results presented in this paper establish a direct correlation between the bulk properties of a self-assembled peptide-based hydrogel and its nanofibrillar network structure. The stiffness of this synthetic, peptide-based hydrogel can be tuned directly by changes in the network density and underlying morphology. Correlation length and fractal exponent trends using SANS and USANS have been verified by direct *in situ* visualization of the network structure under identical concentrations and conditions. Rheological data confirms the bulk property predictions made *via*

a study of the network structure spanning lengthscales from the nanoscale up to the microscale. These hydrogels have been proven to be excellent 2D as well as 3D scaffolds for cell growth and proliferation. Efforts to precisely access the scaffold stiffness range that determine bioproperties such as cell adhesion and motility would undoubtedly provide a complete structure–bioproperty relationship picture for potential *in vivo* usage. In summation, this paper highlights the versatility of peptide chemistry and polymer science to design and characterize advanced materials for specific biological applications.

Experimental

Peptide synthesis and purification

MAX8 was prepared using Fmoc-based solid phase peptide synthesis on a Protein Technologies Sonata Synthesizer. Rink amide resin was used as the solid support with 1H-benzotriazolium-1-[bis(dimethylamino)methylene]-5-chlorohexafluorophosphate-(1-)3-oxide (HCTU) coupling chemistry and 1% 1,8-diazabicyclo[5.4.0]undec-7-ene (DBU), 19% piperidine in 1-methyl-2-pyrrolidone affording Fmoc deprotection. Following synthesis, the peptide was cleaved off the resin as well as side chain deprotected by stirring the resin in a solution of cleavage reagent consisting of 90 : 5 : 3 : 2 trifluoroacetic acid (TFA), thioanisole, ethanedithiol and anisole, respectively. Resin cleavage and side chain deprotection was carried out for 2 hours under a N_2 atmosphere. The resin was separated by filtration and the crude peptide was recrystallized in cold diethyl ether. The crude peptide was purified on a Varian ProStar 320 autoprep using a Vydac C18 peptide/protein semi-preparative, reverse phase HPLC column. Solvents used for performing HPLC consisted of solvent A (0.1% TFA in water) and solvent B (90% acetonitrile, 10% water, 0.1% TFA). MAX8 was purified using an isocratic solvent condition of 0% B for 2 minutes followed by a linear gradient of 0 to 25% solvent B over 7 minutes and an additional linear gradient of 25 to 40% solvent B in 30 minutes and finally a gradient of 40 to 100% solvent B in 5 minutes. Purified peptide fractions collected from HPLC were lyophilized to yield white powder. After lyophilization, the peptide was dissolved in deionized water at a concentration of 1 mg mL^{-1} and re-lyophilized twice to ensure batch-to-batch consistency. The purity of the peptide was determined by analytical HPLC and electrospray ionization-mass spectrometry. Observed $[M + 2\ H]^{+2} = 1116.0$; calculated $[M + 2\ H]^{+2} = 1116.5$.

Hydrogel preparation

2 mg of the peptide were first dissolved in 100 μl milliQ water, resulting in an aqueous peptide solution at room temperature. An equal volume of 100 mM BTP buffer, pH 7.4, 300 mM NaCl was added to the peptide solution to initiate self-assembly. This resulted in a 1 wt% hydrogel. Other concentrations (0.5, 1.5 and 2 wt%) were prepared similarly using appropriate peptide and solvent amounts.

Small angle neutron scattering (SANS)

SANS experiments were performed on the 30 m instrument (NG-3)[49] at the NIST Center for Neutron Research (NCNR), National Institute of Standards and Technology (NIST), Gaithersburg, MD. Gel samples were prepared by mixing the peptide and buffer solutions both prepared in D_2O to enable adequate contrast between the hydrogen-rich gel matrix and the deuterated solvent. Solutions preequilibrated at 5 °C were mixed in a vial and transferred immediately to titanium sample cells with 30 mm diameter quartz windows and a 2 mm path length. All samples were incubated overnight at room temperature prior to scattering measurements. A monochromated neutron beam ($\lambda = 6$ Å) with a wavelength spread ($\Delta\lambda/\lambda$) of 0.14 was incident on the sample. The scattered neutrons were captured on

a 64 cm × 64 cm 2D detector. Varying sample-to-detector distances of 1.33, 4.5 and 13.17 m were used to the study of the scattering wavevector q in the range $0.004 < q$ (Å^{-1}) < 0.4, defined by $q = (4\pi/\lambda) \sin(\theta/2)$, where λ is the neutron wavelength and θ is the scattering angle. Raw data were corrected for background electronic noise and radiation, detector inhomogeneity and sensitivity, and empty cell scattering. Intensities were normalized to an absolute scale relative to main beam transmission measurements through the sample and were reduced according to published protocol.[50] The error bars of the data points for all SANS plots are within the limits of the symbols.

Ultra small angle neutron scattering (USANS)

USANS experiments were performed on the perfect crystal diffractometer (PCD) on beamline BT 5 at the NCNR, NIST. The USANS, a Bonse–Hart-type diffractometer, produces high q-resolution in one direction by using multiple reflections from silicon perfect crystals. A graphite premonochromator is used to select a 2.38 Å neutron wavelength beam. The beam is then diffracted by a three-bounce silicon (220) channel-cut monochromator. After passing through the sample, another three-bounce channel-cut silicon crystal analyzer selects scattering at small angles (θ) in one direction. The data are slit-desmeared as described by Singh *et al.*[51] As with SANS experiments, hydrogels were prepared in D_2O and held in titanium cells with 30 mm diameter quartz windows and a 2 mm pathlength. Experimental time and scattering limitations did not allow data to be obtained in the q-range overlapping the USANS and SANS. Planned hardware improvements will allow this q-range to be assessed during SANS experiments.

Cryogenic transmission electron microscopy (Cryo-TEM)

A thin film (~100 nm) of the pre-assembled MAX8 hydrogel, incubated overnight, was transferred to a lacey carbon grid, blotted with filter paper and plunged into liquid ethane. All samples were prepared using the environmentally controlled, automated Vitrobot from the FEI Company, Hillsboro, OR. In a typical sample preparation, the sample chamber was maintained at 25 °C and 40–50% relative humidity. Prior to plunging in liquid ethane, the sample was blotted with a filter paper 2–3 times for 2 seconds each. Following vitrification, the samples were transferred to a Gatan cryo-holder pre-cooled to −175 °C before inserting into the electron microscope. Imaging was carried out in bright field mode at 120 kV in a Technai T12 electron microscope (FEI Company, Hillsboro, OR). During imaging, the temperature of the sample holder was maintained at −175 °C to inhibit sublimation of vitreous water.

Oscillatory rheology

Rheological experiments were carried out on an Anton Paar MCR 500 rheometer using parallel plate geometry and a 25 mm stainless steel tool. The rheometer was pre-equilibrated at 5 °C. Peptide and buffer solutions, also pre-equilibrated at 5 °C, were mixed in a 1 : 1 ratio, and a 300 μL aliquot was transferred to the rheometer plate. A gap of 500 μm was used for all measurements. S3 standard viscosity mineral oil (Viscosity at 20 °C = 4.013 mPa s) was placed around the sample to prevent water evaporation over time. In a typical experiment, the temperature was increased from 5 to 20 °C over 100 s causing the peptide solution to gel on the rheometer. The temperature was subsequently maintained at 20 °C for 1 hour during a dynamic time sweep experiment performed at an angular frequency of 6 rad s^{-1} and a strain of 0.2%. Mean G' observed at the end of 1 hour from 3 independent experiments on 3 discreet samples shows a standard deviation of less than 10%. Frequency sweeps from 0.1 to 100 rad s^{-1} and amplitude sweeps from 0.01 to 100% strain were

subsequently performed to assess the frequency dependence and the linear viscoelastic region, respectively.

Cell maintenance

MC3 T3-E1 (preosteoblasts) cells were purchased from American Type Culture Collection (ATCC) and routinely cultured in alpha minimum essential media (αMEM) without ascorbic acid and supplemented with 10% fetal bovine serum (FBS), 1% penicillin–streptomycin antibiotics at 37 °C with 95% relative humidity and 5% CO_2. Medium was replaced every 2–3 days and confluent cells were subcultured through trypsinisation.

Hydrogel preparation for cell culture

0.5 mg MAX8 was dissolved in 50 μL deionized water in a glass vial. The peptide solution was transferred to an 8 well glass chamber. 50 μL BTP buffer (at pH 7.4) was then added to the well to yield a 0.5 wt% hydrogel. The hydrogel was left in the incubator at 37 °C with 95% relative humidity and 5% CO_2, for 2 hours. After this period 100 μL of αMEM (without FBS) was added on top, to prepare the pre-formed hydrogel for cell culture. The same procedure was employed for 1, 1.5 and 2 wt% hydrogels. Media was aspirated before cell seeding. MC3 T3 preosteoblast cells were suspended in cell culture media at a concentration of about 40 000 cells mL^{-1}, and 400 μL of this suspension was added on the pre-formed hydrogels. The cells were cultured in the incubator for 24 hours before examination under laser scanning confocal microscope.

Cell viability

After 24 hours of cell culture on hydrogel scaffolds, a 2 mM solution of calcein acetoxymethylester (calcein AM, cytoplasmic dye) and a 4 mM solution of propidium iodide (PI, nuclear stain) in αMEM were used to stain live and dead cells, respectively, and were observed with confocal microscopy (LSCM, Zeiss LSM 510 NLO). The cytoplasm of live cells are distinguished by their green appearance whereas the nuclei of dead cells appear red. Tissue culture treated polystyrene (TCTP) was used as positive control.

Actin localization

The cytoskeletal organization of MC3 T3 preosteoblast cells was examined by labeling F-actin microfilaments with a fluorescently labeled Alexa Fluor® 568 phalloidin dye. MC3 T3 preosteoblast cells were suspended in culture media with density of 50 000 cells mL^{-1}. A 200 μL aliquot of cell suspension was added to 0.75 wt% hydrogel prepared in 8-well glass chamber and maintained under culturing conditions. After 24 hours, cells were washed three times with phosphate buffered saline (PBS), fixed with 4% paraformaldehyde for 15 minutes, and washed with PBS three times. Actin filaments were stained with 1 μL mL^{-1} of 6.6 μM Alexa Fluor® 568 dye in PBS, for 1 hour, followed by three times washing with PBS. 1 μL mL^{-1} of Syto® 13 in PBS was added to samples for nuclear staining. Cells were imaged with LSCM.

Acknowledgements

Financial support for this work was obtained through the Small Angle Neutron Scattering on Polymers and Complex Fluids Award (US Department of Commerce, #70NANB7H6178), Hydrogels from Designed Peptides Award (National Institutes of Health, RO1 DE016386) and the NSF Career Award #0348323. RAH is grateful to Dr Boualem Hammouda at NCNR-NIST for stimulating discussions.

References

1 B. Jeong, Y. H. Bae, D. S. Lee and S. W. Kim, Biodegradable block copolymers as injectable drug-delivery systems, *Nature*, 1997, **388**(6645), 860.
2 D. A. LaVan, Small-scale systems for *in vivo* drug delivery, *Nat. Biotechnol.*, 2003, **21**, 1184–1191.
3 J. Li, X. Li, X. Ni, X. Wang, H. Li and Z. Zhou, Injectable supramolecular hydrogels self-assembled by polymers and cyclodextrins for controlled drug delivery, *Key Eng. Mater.*, 2005, **288**, 117–120.
4 K. Y. Lee and D. J. Mooney, Hydrogels for tissue engineering, *Chem. Rev.*, 2001, **101**(7), 1869–79.
5 Y. Takimoto, V. Dixit, M. Arthur and G. Gitnick, *De novo* liver tissue formation in rats using a novel collagen-polypropylene scaffold, *Cell Transplant.*, 2003, **12**(4), 413–21.
6 S. J. Bryant, R. J. Bender, K. L. Durand and K. S. Anseth, Encapsulating chondrocytes in degrading PEG hydrogels with high modulus: Engineering gel structural changes to facilitate cartilaginous tissue production, *Biotechnol. Bioeng.*, 2004, **86**(7), 747–755.
7 H.-W. Kim, H.-E. Kim and V. Salih, Stimulation of osteoblast responses to biomimetic nanocomposites of gelatin–hydroxyapatite for tissue engineering scaffolds, *Biomaterials*, 2005, **26**(25), 5221.
8 C. A. Simmons, E. Alsberg, S. Hsiong, W. J. Kim and D. J. Mooney, Dual growth factor delivery and controlled scaffold degradation enhance *in vivo* bone formation by transplanted bone marrow stromal cells, *Bone*, 2004, **35**(2), 562–9.
9 T. A. Holland, E. W. Bodde, L. S. Baggett, Y. Tabata, A. G. Mikos and J. A. Jansen, Osteochondral repair in the rabbit model utilizing bilayered, degradable oligo(poly(ethylene glycol)fumarate) hydrogel scaffolds, *J. Biomed. Mater. Res., A*, 2005, **75**, 156.
10 R. A. Hule and D. J. Pochan, Polymer nanocomposites for biomedical applications, *MRS Bull.*, 2007, **32**, 354–358.
11 J. L. Drury and D. J. Mooney, Hydrogels for tissue engineering: scaffold design variables and applications, *Biomaterials*, 2003, **24**(24), 4337.
12 G. Miquelard-Garnier, S. Demoures, C. Creton and D. Hourdet, Synthesis and rheological behavior of new hydrophobically modified hydrogels with tunable properties, *Macromolecules*, 2006, **39**(23), 8128–8139.
13 M. Matsusaki, H. Yoshida and M. Akashi, The construction of 3D-engineered tissues composed of cells and extracellular matrices by hydrogel template approach, *Biomaterials*, 2007, **28**(17), 2729–2737.
14 R. Zhang, M. Tang, A. Bowyer and R. Eisenthal, A novel pH- and ionic-strength-sensitive carboxy methyl dextran hydrogel, *Biomaterials*, 2005, **26**(22), 4677–4683.
15 J. D. Hartgerink, Nanomedicine: New material stops bleeding in a hurry, *Nature*, 2006, **1**(3), 166–167.
16 T. J. Sanborn, P. B. Messersmith and A. E. Barron, *In situ* crosslinking of a biomimetic peptide–PEG hydrogel *via* thermally triggered activation of factor XIII, *Biomaterials*, 2002, **23**(13), 2703–10.
17 K. T. Nguyen and J. L. West, Photopolymerizable hydrogels for tissue engineering applications, *Biomaterials*, 2002, **23**(22), 4307–4314.
18 H. J. Lee, J. S. Lee, T. Chansakul, C. Yu, J. H. Elisseeff and S. M. Yu, Collagen mimetic peptide-conjugated photopolymerizable PEG hydrogel, *Biomaterials*, 2006, **27**(30), 5268–5276.
19 R. P. Nagarkar, R. A. Hule, D. J. Pochan and J. P. Schneider, *De novo* synthesis of strand-swapped β-hairpin hydrogels, *J. Am. Chem. Soc.*, 2008, **130**(13), 4466–4474.
20 J. P. Schneider, D. J. Pochan, B. Ozbas, K. Rajagopal, L. Pakstis and J. Kretsinger, Responsive hydrogels from the intramolecular folding and self-assembly of a designed peptide, *J. Am. Chem. Soc.*, 2002, **124**(50), 15030–15037.
21 D. J. Pochan, J. P. Schneider, J. Kretsinger, B. Ozbas, K. Rajagopal and L. Haines, Thermally reversible hydrogels *via* intramolecular folding and consequent self-assembly of a *de novo* designed peptide, *J. Am. Chem. Soc.*, 2003, **125**(39), 11802–11803.
22 B. Ozbas, J. Kretsinger, K. Rajagopal, J. P. Schneider and D. J. Pochan, Salt-triggered peptide folding and consequent self-assembly into hydrogels with tunable modulus, *Macromolecules*, 2004, **37**(19), 7331–7337.
23 L. A. Haines, K. Rajagopal, B. Ozbas, D. A. Salick, D. J. Pochan and J. P. Schneider, Light-activated hydrogel formation *via* the triggered folding and self-assembly of a designed peptide, *J. Am. Chem. Soc.*, 2005, **127**(48), 17025–17029.
24 J. K. Kretsinger, L. A. Haines, B. Ozbas, D. J. Pochan and J. P. Schneider, Cytocompatibility of self-assembled β-hairpin peptide hydrogel surfaces, *Biomaterials*, 2005, **26**, 5177–5186.

25 L. Haines-Butterick, K. Rajagopal, M. Branco, D. Salick, R. Rughani, M. Pilarz, M. S. Lamm, D. J. Pochan and J. P. Schneider, Controlling hydrogelation kinetics by peptide design for three-dimensional encapsulation and injectable delivery of cells, *Proc. Natl. Acas. Sci. U. S. A.*, 2007, **104**(19), 7791–7796.
26 G. Porod, General Theory, in *Small Angle X-ray Scattering*, ed. O. Glatter and O. Kratky, Academic Press: London, 1982, pp. 46–48.
27 B. Hammouda, Solvation characteristics of a model water-soluble polymer, *J. Polym. Sci., Part B: Polym. Phys.*, 2006, **44**(22), 3195–3199.
28 B. Hammouda, D. L. Ho and S. Kline, Insight into clustering in poly(ethylene oxide) solutions, *Macromolecules*, 2004, **37**(18), 6932–6937.
29 B. Hammouda, F. Horkay and M. L. Becker, Clustering and solvation in poly(acrylic acid) polyelectrolyte solutions, *Macromolecules*, 2005, **38**(5), 2019–2021.
30 L. Pakstis, R. A. Hule, A. P. Nowak, T. J. Deming and D. J. Pochan, Morphology and assembly of amphiphilic diblock copolypeptides revealed through small angle and ultra small angle neutron scattering; to be submitted.
31 R. A. Hule, R. P. Nagarkar, B. Hammouda, J. P. Schneider and D. J. Pochan, Fractal nature of semiflexible networks in β-hairpin peptide hydrogels; to be submitted.
32 S. Ramachandran, J. Trewhella, Y. Tseng and Y. B. Yu, Coassembling peptide-based biomaterials: effects of pairing equal and unequal chain length oligopeptides, *Chem. Mater.*, 2006, **18**(26), 6157–6162.
33 H. D. Bale and P. W. Schmidt, Small-angle X-ray-scattering investigation of submicroscopic porosity with fractal properties, *Phys. Rev. Lett.*, 1984, **53**(6), 596–599.
34 S. Koizumi, M. Annaka, S. Borbely and D. Schwahn, Fractal structures of a poly(*N*-isopropylacrylamide) gel studied by small-angle neutron scattering over a *Q*-range from 10–5 to 0.1 A^{-1}, *Physica B*, 2000, **276–278**, 367.
35 B. Hammouda and D. Worcester, The denaturation transition of DNA in mixed solvents, *Biophys. J.*, 2006, **91**(6), 2237.
36 M. Shibayama, F. Ikkai, S. Inamoto, S. Nomura and C. C. Han, pH and salt concentration dependence of the microstructure of poly(*N*-isopropylacrylamide-co-acrylic acid) gels, *J. Chem. Phys.*, 1996, **105**, 4358.
37 M. Crichton and S. Bhatia, Structure and intermicellar interactions in block polyelectrolyte assemblies, *J. Appl. Crystallogr.*, 2003, **36**(3), 652–655.
38 S. R. Bhatia, Ultra-small-angle scattering studies of complex fluids, *Curr. Opin. Colloid Interface Sci.*, 2005, **9**(6), 404–411.
39 R. J. Pelham Jr and Y.-l. Wang, Cell locomotion and focal adhesions are regulated by substrate flexibility, *Proc. Natl. Acad. Sci. U. S. A.*, 1997, **94**(25), 13661–13665.
40 M. M. Stevens and J. H. George, Exploring and engineering the cell surface interface, *Science*, 2005, **310**(5751), 1135–1138.
41 D. E. Discher, P. Janmey and Y.-l. Wang, Tissue Cells feel and respond to the stiffness of their substrate, *Science*, 2005, **310**(5751), 1139–1143.
42 A. J. Engler, S. Sen, H. L. Sweeney and D. E. Discher, Matrix elasticity directs stem cell lineage specification, *Cell*, 2006, **126**(4), 677.
43 A. J. Engler, M. A. Griffin, S. Sen, C. G. Bonnemann, H. L. Sweeney and D. E. Discher, Myotubes differentiate optimally on substrates with tissue-like stiffness: pathological implications for soft or stiff microenvironments, *J. Cell Biol.*, 2004, **166**(6), 877–887.
44 H. R. Ramay, J. P. Schneider and D. J. Pochan, Self-assembling peptide hydrogel for osteogenic cell culture; to be submitted.
45 A. J. Garcia and C. D. Reyes, Bio-adhesive surfaces to promote osteoblast differentiation and bone formation, *J. Dent. Res.*, 2005, **84**(5), 407–413.
46 F. G. Giancotti, Integrin signaling, *Science*, 1999, **285**(5430), 1028–1033.
47 B. Geiger, A. Bershadsky, R. Pankov and K. M. Yamada, Transmembrane crosstalk between the extracellular matrix and the cytoskeleton, *Nat. Rev. Mol. Cell Biol.*, 2001, **2**(11), 793.
48 S. K. Sastry and K. Burridge, Focal adhesions: A nexus for intracellular signaling and cytoskeletal dynamics, *Exp. Cell Res.*, 2000, **261**(1), 25–36.
49 C. J. Glinka, J. G. Barker, B. Hammouda, S. Krueger, J. J. Moyer and W. J. Orts, The 30 m small-angle neutron scattering instruments at the National Institute of Standards and Technology, *J. Appl. Crystallogr.*, 1998, **31**, 430–445.
50 S. R. Kline, Reduction and analysis of SANS and USANS data using IGOR Pro, *J. Appl. Crystallogr.*, 2006, **39**, 895–900.
51 M. A. Singh, S. S. Ghosh and R. F. Shannon Jr, A direct method of beam-height correction in small-angle X-ray scattering, *J. Appl. Crystallogr.*, 1993, **26**, 787–794.

